Crossover from impurity to valence band in diluted magnetic semiconductors: Role of Coulomb attraction by acceptors

F. Popescu,[1,*] C. Şen,[1,2] E. Dagotto,[3,4] and A. Moreo[3,4]
[1]*Department of Physics, Florida State University, Tallahassee, Florida 32306, USA*
[2]*National High Magnetic Field Laboratory, Tallahassee, Florida 32310, USA*
[3]*Department of Physics and Astronomy, University of Tennessee, Knoxville, Tennessee 37996, USA*
[4]*Materials Science and Technology Division, Oak Ridge National Laboratory, Oak Ridge, Tennessee 32831, USA*
(Received 1 May 2007; published 15 August 2007)

The crossover between an impurity band (IB) and a valence band (VB) regime as a function of the magnetic impurity concentration in a model for diluted magnetic semiconductors (DMSs) is studied systematically by taking into consideration the Coulomb attraction between the carriers and the magnetic impurities. The density of states and the ferromagnetic transition temperature of a spin-fermion model applied to DMSs are evaluated using dynamical mean-field theory and Monte Carlo (MC) calculations. It is shown that the addition of a square-well-like attractive potential can generate an IB at small enough Mn doping x for values of the p-d exchange J that are not strong enough to generate one by themselves. We observe that the IB merges with the VB when $x \geqslant x_c$ where x_c is a function of J and the Coulomb strength V. Using MC simulations, we demonstrate that the range of the Coulomb attraction plays an important role. While the on-site attraction, which has been used in previous numerical simulations, effectively renormalizes J for all values of x, an unphysical result, a nearest-neighbor range attraction renormalizes J only at very low dopings, i.e., until the bound holes wave functions start to overlap. Thus, our results indicate that the Coulomb attraction can be neglected to study Mn-doped GaSb, GaAs, and GaP in the relevant doping regimes, but it should be included in the case of Mn-doped GaN, which is expected to be in the IB regime.

DOI: 10.1103/PhysRevB.76.085206 PACS number(s): 75.50.Pp, 71.10.−w, 71.55.Eq

I. INTRODUCTION

The development of spintronics devices[1] has motivated a large body of research on diluted magnetic semiconductors[2,3] with the ultimate aim of creating materials with Curie temperatures (T_C) above room temperature. This ambitious goal can only be achieved by a detailed understanding of the underlying mechanisms that govern the behavior of currently available diluted magnetic semiconductors (DMSs).

Most theoretical approaches to study these materials start with one of two extreme regimes: (i) the limit of high Mn doping in which holes are directly doped into the valence band (VB) and, thus, are uniformly distributed in the sample[2–4] (VB scenario) and (ii) the limit of very low Mn doping in which holes are electrically bound to the impurity cores and an impurity band (IB) develops due to wave function overlap as the number of holes increases[5] (IB scenario). Researchers using the VB limit claim that it is valid for all relevant dopings—namely, $x > 1\%$ in $Ga_{1-x}Mn_xAs$—and some experimental results support their view.[6,7] However, a similar claim is advanced by the groups promoting the IB scenario—i.e., that the IB exists up to the largest value of x that has been reached experimentally ($x \approx 10\%$). This view also appears supported by the analysis of some experimental data.[8,9]

To solve this apparent puzzle, it is very important to study theoretically the DMS problem using unbiased techniques that provide reliable estimations for the value of x where the IB to VB crossover takes place. By "unbiased" we mean approaches that do not make further assumptions on the properties of the ground state, such as that the holes are uniformly distributed or that an IB exists, once a Hamiltonian is proposed. Such unbiased approaches could be provided by numerical nonperturbative techniques: in fact, the Monte Carlo (MC) and dynamical mean-field theory (DMFT) methods have already been applied to a variety of phenomenological models for the DMSs.[10–14] These previous studies have been able to determine a crossover between the VB and IB behaviors, but only as a function of increasing values of the p-d exchange J. However, most experimental results appear to indicate that the realistic J for (Ga,Mn)As is approximately 1 eV,[15] which corresponds to the weak coupling regime in which no IB is generated by J alone. In fact, recent results obtained applying MC techniques to a six-orbital microscopic model, in which both the correct lattice geometry and the spin-orbit interactions were considered, indicate that (Ga,Mn)As is indeed in the VB regime for $x \gtrsim 3\%$.[16] In addition, DMFT techniques, which allow for the study of the very diluted ($x \ll 1$) regime, have shown that for values of J in the weak coupling region, an IB never develops as a function of x.[11–14] However, experiments based on electron paramagnetic resonance,[17] infrared spectroscopy,[18] and magnetization measurements[19] of the electronic structure of one Mn ion doped in GaAs have actually shown the existence of a hole state with binding energy $E_b = 112.4$ meV centered at the $S = 5/2$ Mn ion. Moreover, analytical studies indicated that E_b has contributions from *both* the spin-dependent p-d hybridization and the Coulomb attraction between the hole and the Mn trapping center.[20] When additional Mn ions are added, the wave functions of the bounded holes will start overlapping and an IB will develop. Further increasing x should widen the IB, locating it closer to the VB and eventually a regime of complete hybridization with the holes doped into the VB is expected to occur. Thus, it is clear

that a crossover from the IB to the VB regime should take place in (Ga,Mn)As as a function of x.

In this paper, it will be argued that an IB-VB crossover will be missed in theoretical studies of materials with a weak J if the Coulomb attraction is disregarded, while materials with very strong J will be in the IB regime regardless of doping. In fact, here we explicitly show that by the simultaneous consideration of J and V in the formalism, the experimentally observed transition from IB to VB with increasing x can be understood. The organization of the paper is the following: in Sec. II the nonmagnetic interactions in DMSs are described; the model used and the DMFT technique are presented in Sec. III; in Sec. IV the results, including MC simulations, are discussed; and Sec. V is devoted to the conclusions.

II. SPIN-INDEPENDENT INTERACTIONS BETWEEN HOLES AND MAGNETIC IMPURITIES

As remarked in the Introduction, most of the numerical work on DMSs has been performed on models that focused on the role of the spin-dependent p-d exchange J interaction between the spins of the localized impurities and the doped holes.[10–12] This is certainly sufficient to capture qualitatively many of the properties of these compounds, including the generation of ferromagnetism. However, nonmagnetic interactions between holes and impurities must be considered in order to improve the quantitative agreement with experiments. This additional potential term in the model has been generally referred to as "chemical disorder" (V),[21] and it summarizes all the nonmagnetic interactions between the localized impurities and the holes. In this context, Tworzydlo [21] used a short-range potential (less than nearest-neighbor range) with a square-well form of depth V_0 and considered both positive (repulsive) and negative (attractive) values of V_0. The potential was introduced to explain an apparent x dependence of the p-d exchange in $Cd_{1-x}Mn_xS$. Dietl[22] recently used the same approach to address apparently contradictory experimental results for $Ga_{1-x}Mn_xN$. He also pointed out[23] that this kind of extra potential term leads to a chemical shift in the standard impurity language, or to a valence band offset in the alloy nomenclature, and that J and V are actually related[22,24] through the expression $V/J=5(U_{\text{eff}}+2\epsilon_d)/4U_{\text{eff}}$ where U_{eff} is an effective correlation energy for the $3d$ shell and ϵ_d is its energetic position with respect to the top of the valence band. However, the value of V is not easy to determine and, thus, it has been added as an extra free parameter by some authors (with V allowed to take both positive and negative values).[14,25,26] Other efforts focused just on the attractive Coulomb interaction between the holes and the impurities.[13,20,27]

Only some of the previously mentioned investigations have attempted to study the effects of the Coulomb attraction at finite x with unbiased techniques. The authors of Ref. 20 studied the case of a single Mn impurity, considering the long-range Coulomb potential supplemented by a central cell correction with a Gaussian or square-well shape, which is routinely introduced in calculations of bound-state energies for impurities in semiconductors.[28] For higher dopings, it is believed that the most important Coulombic term is the central-cell contribution since the long-range potential is screened. In Ref. 13, the coherent potential approximation (CPA), very similar in spirit to DMFT, was applied to a single-orbital model which included both the spin-dependent p-d hybridization J and an on-site central-cell Coulomb attraction V. It was claimed that the IB-VB crossover for (Ga,Mn)As using $V=0.6$ eV (chosen to reproduce, in combination with $J=0.8$ eV, the single-impurity bound-state energy) should occur for $x\sim 1\%-3\%$. While in Ref. 26 a repulsive on-site potential was added, both the repulsive and attractive cases were considered in Ref. 14. However, these important previous efforts did not present a systematic analysis of results as a function of J, V, and x, which is part of the goals of the present study.

In this work we apply DMFT to a model that includes J and the Coulomb attraction V. The density of states (DOS) and T_C are studied in a wide range of couplings, hoppings, carrier fillings p, and Mn concentrations x, and estimations of the most appropriate values for different materials are made. We obtain the IB-VB crossover for a large class of DMSs and show that with a suitable strength V included, the IB regime can always be reached by decreasing the Mn concentration.

III. MODEL AND DMFT FORMALISM

The spin-fermion Hamiltonian used here and in several previous studies contains a kinetic t term that describes the hopping of holes between two neighboring i and j lattice sites (t is set to 1 to define the energy unit), an exchange interaction J_H term that anti-aligns the carrier's spin with the magnetic moment of the impurity (considered classical) at site I, and a V term that takes into account the on-site central-cell part of the attractive Coulomb potential,[29]

$$\mathcal{H}=-t\sum_{\langle ij\rangle,\alpha}(c^{\dagger}_{i\alpha}c_{j\alpha}+\text{H.c.})+2J_H\sum_I \mathbf{S}_I\cdot\mathbf{s}_I-V\sum_I n_I. \quad (1)$$

Here, $c^{\dagger}_{i\alpha}$ ($c_{i\alpha}$) is the creation (destruction) operator for a hole with spin α at site i, $\mathbf{s}_i=c^{\dagger}_{i\alpha}\boldsymbol{\sigma}_{\alpha\beta}c_{i\beta}/2$ is the hole's spin, $\mathbf{S}_I=S\mathbf{m}_I$ is the classical spin of the local moment, and n_I is the number of holes at I.

Several details of the DMFT calculations were already presented in Ref. 11 for the case $V=0$; thus, here only a brief summary is given and the modifications introduced by a nonzero V are remarked on. DMFT uses the momentum independence of the self-energy in infinite dimensions [$\Sigma(\mathbf{p},i\omega_n)\rightarrow\Sigma(i\omega_n),\omega_n=(2n+1)\pi T$] (Ref. 30) and reproduces the physics of diluted correlated systems in lower dimensions.[31] Within DMFT, the bare Green's function $G_0(i\omega_n)$ contains all the information about the hopping of carriers onto and off magnetic (with probability x) and nonmagnetic (with probability $1-x$) sites. With Eq. (1) the full Green's function $G(i\omega_n)$ is solved by integration, obtaining

the result $\langle G(i\omega_n)\rangle = x\langle [G_0^{-1}(i\omega_n) + J\mathbf{m}\hat{\sigma} + V\hat{\mathbf{I}}]^{-1}\rangle + (1-x)\times\langle G_0(i\omega_n)\rangle$, where $J = J_H S$.[32] This equation, complemented with the relation $\langle G_0^{-1}(i\omega_n)\rangle = z_n - (W^2/16)\langle G(i\omega_n)\rangle$ valid within the assumption of a Bethe lattice,[33] can be solved with a semicircular noninteracting $\mathrm{DOS}(\omega) = 2\,\mathrm{Re}\sqrt{(W/2)^2 - \omega^2}/\pi W$ ($z_n = \mu + i\omega_n$, μ is the chemical potential, and $W = 4t$ is the bandwidth). Being spin diagonal, $\langle G_0\rangle$ and $\langle G_0^{-1}\rangle$ are expanded in powers of σ_z as $\langle\alpha\rangle = \alpha_0\hat{\mathbf{I}} + \Sigma_k \alpha_k \sigma_z^k$, where $\alpha_k \sim M^k$, M being the order parameter used to detect the ferromagnetic (FM) transition. To linear order in M we write $\langle G_0^{-1}(i\omega_n)\rangle = B(i\omega_n)\hat{\mathbf{I}} + Q(i\omega_n)\sigma_z$ and then $B(i\omega_n)$ is found from a fourth-order equation

$$B_\pm = z_n - x\frac{W^2}{16}\frac{[B_\pm + V \pm JM]}{[B_\pm + V]^2 - J^2} - (1-x)\frac{W^2}{16}\frac{1}{B_\pm}, \tag{2}$$

which at $\mu = 0$ and with $i\omega_n \to \omega$ gives us the low-temperature interacting $\mathrm{DOS}_\pm(\omega) = -\mathrm{Im}[B_\pm(\omega)]/\pi$ for up (+) and down (−) spin configurations.[34] The expression for $Q(i\omega_n)$,

$$Q = x\frac{W^2}{16}\left\{\frac{Q + JM}{(B+V)^2 - J^2} + \frac{2J^2 Q/3}{[(B+V)^2 - J^2]^2}\right\} + (1-x)\frac{W^2}{16}\frac{Q}{B^2}, \tag{3}$$

leads us to an implicit equation for T_C in the form

$$-\sum_{n=0}^{\infty}\frac{4xW^2J^2B^2}{[48B^2 - 3(1-x)W^2]\{[B+V]^2 - J^2\}^2 - 3xW^2B^2\{[B+V]^2 - J^2\} - 2xW^2J^2B^2} = 1, \tag{4}$$

where $B(i\omega_n)$ is given by Eq. (2) at $M = 0$. The T_C contained in ω_n can be obtained from Eq. (4) numerically.

IV. RESULTS

A. General analysis

Let us start the discussion of results by considering the general dependence of a variety of quantities with the parameters of the model. The DOS obtained from Eq. (2) at $x = 0.035$ is displayed in Fig. 1 for various values of J, M, and V. As observed in Fig. 1(a), the J term alone is able to generate an IB but only if J/W exceeds a critical value $J_c/W \sim 0.35$. At realistic couplings for (Ga,Mn)As (namely, $J/W \cong 0.25$ if we assume $J \approx t \sim 1$ eV) there is no IB generated by the J term alone. However, with the addition of Coulomb attraction, when a value $V/W \geqslant 0.125$ is reached, then a well-defined split IB forms, as shown in Fig. 1(b). No "symmetric" impurity band exists at high energies since the observed one is due to the carriers that are trapped in the vicinity of the core spins through the influence of V and are fully aligned for $M = 1$ [Fig. 1(c)]. The growth of J/W produces asymmetric low- and high-energy impurity bands if $V \neq 0$ [Fig. 1(d)].

We have observed that the coupling strength J_c/W for which the IB develops is a function of x; namely, the larger x is, the larger J_c/W becomes. Thus, we used Eq. (2) to draw the phase diagram J_c/W vs x at various values of V. When $V = 0$ the occurrence of an IB due only to the J term requires a $J_c/W \approx 0.25$ when $x \to 0$, as seen in Fig. 2(a). When $x \to 0$ and $J/W < 0.25$ the addition of a potential V leads to the relation $(J+V)/W \approx 0.25$ to establish the boundary of the region where an IB develops. Our calculations also show that the boundary between the IB and VB regions in the full J-x plane just moves down by an amount $\Delta(V)$ after the introduction of the Coulomb attraction. This $\Delta(V)$ is independent of x, indicating that $J_c(x,V) = J_c(x,V=0) - \Delta(V)$ as can be seen in Fig. 2(a).[35] This means that an IB will be generated by a $J < J_c(x,V=0)$ if a V such that $(J+V)/W \approx J_c(x)/W|_{V=0}$ is added. Then, intuitively the effect of the addition of V is to renormalize J to a larger value. This result is not surprising because J has a dual effect: (i) it induces ferromagnetism, but (ii) it also tends to localize the holes near the impurity so that they take advantage of the antifer-

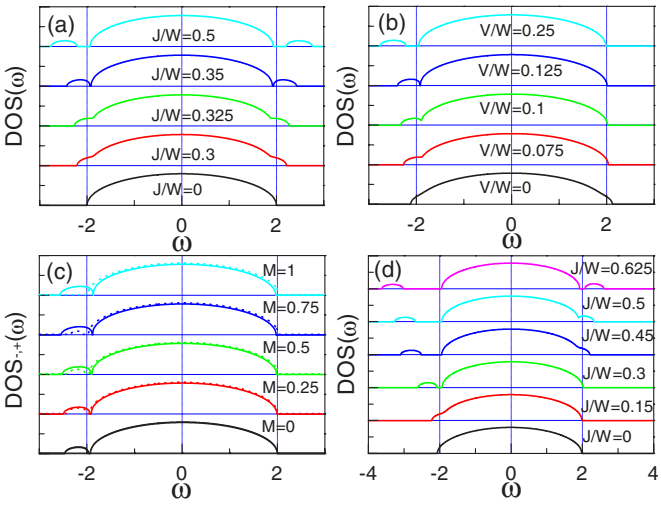

FIG. 1. (Color online) (a) DMFT low-temperature DOS at $V = 0$, $M = 0$, and different values of J/W. An IB forms if J/W exceeds a critical value ≈ 0.35. (b) DOS at $M = 0$, $J/W = 0.25$ [believed to be realistic for (Ga,Mn)As], and different values of V/W. An IB forms if $V/W \geqslant 0.125$. (c) Same as in (b) but at $V/W = 0.125$ and for several values of M. The solid curve corresponds to DOS_- while the dotted curve is for DOS_+. (d) DOS at $M = 0$, $V/W = 0.15$, and various J/W. With a $V/W \neq 0$ the electron-hole symmetry is lost. In all frames the DOS is in arbitrary units and $x = 0.035$. At $x = 0.05$ we have reproduced the DOS obtained in Ref. 13 with the CPA.

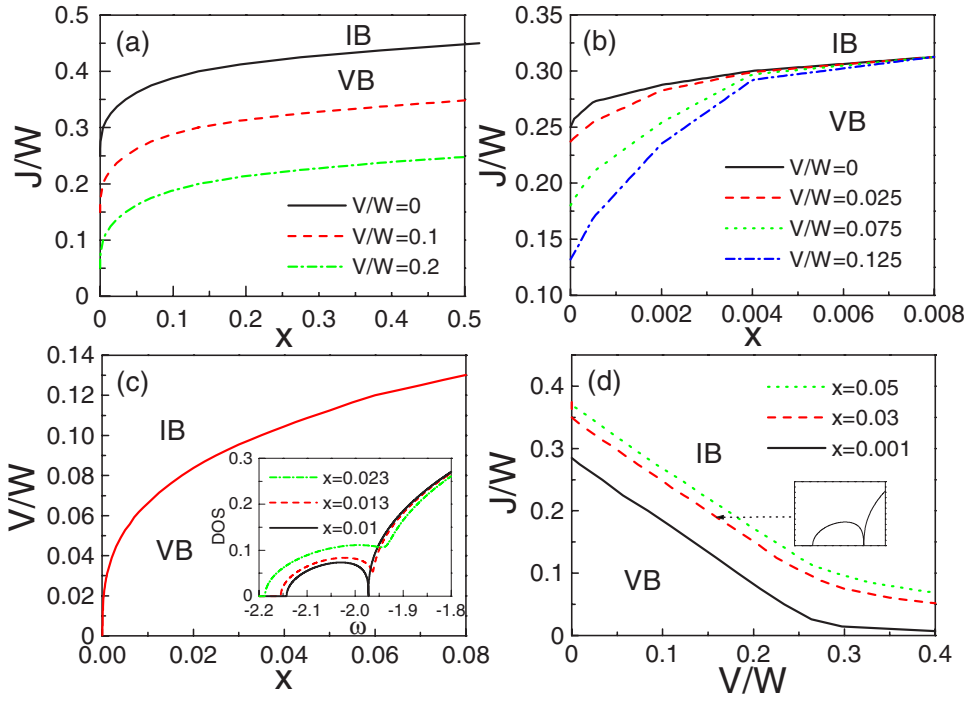

FIG. 2. (Color online) (a) The diagram J/W vs x for various values of V. The solid curve defines the IB-VB crossover at $V=0$. (b) The diagram J/W vs x for (Ga,Mn)As when V is x dependent. The $V\neq 0$ curves all join at $x\approx 0.005$, which marks the Mn doping concentration beyond which the Coulomb attraction is no longer relevant and the IB disappears for realistic couplings. (c) The diagram V/W vs x at a realistic ratio for (Ga,Mn)As $J/W=0.25$ with an on-site Coulomb attraction. The inset shows the merging of the impurity and valence bands with increasing x, at $V/W=0.066$. (d) The diagram J/W vs V/W at various x. The inset shows the DOS at $J/W=0.2$, $V/W=0.148$, and $x=0.03$. Since J_c/W is x dependent, the VB "triangle" shrinks (expands) as x decreases (increases), with the shrinking saturating at $J_c/W\rightarrow 0.25$.

romagnetic coupling. This last property is similar to the effect produced by the Coulomb attraction V. However, it would be expected that as x increases and more holes are added to the system, the wave functions of the holes will start to overlap, and as the holes become delocalized, the effect of V should become less important. Thus, we would expect that the crossover boundaries between the IB and VB regions indicated in Fig. 2(a) should become closer to the $V=0$ curve as x increases, instead of remaining parallel as in the figure. Similar results are observed in MC simulations.[36] We believe that the reason for this unexpected behavior is related to the fact that here an on-site central-cell potential is being considered. This behavior can be corrected by considering a nearest-neighbor-range potential[36] or, within the DMFT framework, by considering a phenomenological on-site potential that depends on x such as

$$V(x) = V\exp\{-(x/x_0)^2\}, \tag{5}$$

where x_0 can be roughly estimated using Mott's criterion[37] as

$$x_0 = \frac{0.25^3}{4}\left(\frac{a_0}{a_B}\right)^3, \tag{6}$$

with a_0 being the side of the cubic cell of the material and a_B the Bohr radius for the bound impurity. For a material such as (Ga,Mn)As, which has an estimated $a_B\sim 8$ Å, we obtain $x_0=0.0014$. The resulting boundary between the IB and VB regions is presented in Fig. 2(b) which indicates that for realistic values of J (0.2 W) and V_0 (0.1 W) for (Ga,Mn)As, the crossover would occur for $x<0.5\%$.

After having remarked that some paradoxes of the results can be solved by extending the size range of the attraction or, similarly, by reducing its strength with increasing x, here we will continue the discussion of the qualitative aspects for the case of the on-site central-cell potential. The main reason for it is to be able to compare our conclusions with previous results in the literature since an on-site potential is the only approach used in previous numerical investigations.[13,14] There are still some quantitative aspects that may need the x-dependent potential of the previous paragraphs, and those will be clarified below.

Focusing on the on-site potential, it can be observed that even if $J/W<J_c/W$, the IB regime can in general be reached either by increasing V at fixed x or by decreasing x at fixed V [see Fig. 2(c)]. While at $x\rightarrow 0$ the carriers trapped due to V in the vicinity of each Mn core spin reside in an impurity-like bound state, as x increases the wave functions that describe the bound state at the manganeses start overlapping (due to the combined effects of V and J), producing an IB that at a critical x_c merges with the VB. The renormalization condition obtained in our calculations yields an IB-VB boundary in the diagram J/W vs V/W, for a fixed x, as shown in Fig. 2(d). This boundary deviates from linear only for very small values of J/W which is not a physically interesting region. According to the results in Fig. 2(d) the area of the VB region is a minimum for $x\rightarrow 0$ and increases with increasing x.

TABLE I. DMFT calculated values of V that produce a bound state with energy E_b for the values of J and bandwidth W shown corresponding to the indicated DMSs. The calculated doping density x_c ($\tilde{x}_c$) at which the IB-VB crossover occurs for an x-independent (dependent) potential is listed. The IB label indicates that the material is in the IB regime at all $x \in (0,1]$. Values of a_0, a_B, and x_0 (see text) for each material are also shown.

Material	J (eV)	E_b (eV)	W (eV)	V (eV)	x_c (%)	a_0 (Å)	a_B (Å)	x_0	$\tilde{x}_c$ (%)
(Ga,Mn)N	2.5	1.4	10	2.7	IB	4.42	1.6	0.082	7.2
			8	2.014	IB				9.3
			6	1.31	IB				21
			4	0.47	IB				IB
(Ga,Mn)P	1.34	0.41	10	2.4	5.2	5.45	4.5	0.007	0.422
			8	1.786	8.3				0.493
			6	1.173	16.7				0.637
			4	0.525	30				2.14
(Ga,Mn)As	1.2	0.112	10	1.883	0.52	5.65	8	0.0014	0.059
			8	1.324	0.85				0.068
			6	0.761	1.35				0.09
			4	0.19	3.1				0.37
(Ga,Mn)Sb	0.96	0.016	10	1.74	0.025	6.10	39	0.00015	0.00044
			8	1.232	0.045				0.00053
			6	0.698	0.064				0.00065
			4	0.175	0.13				0.0014

B. Specific results for (Ga,Mn)As and other compounds

The literature does not provide a unique value of V for the case of (Ga,Mn)As. The main reason is that the value of V that generates a bound state upon doping by one hole is a function of both J and the bandwidth W, as can be observed from the results presented in Table I. Thus, in Ref. 20 a value of $V=2.3$ eV is determined for $J=0.9$ eV with $W \approx 10$ eV since a Luttinger-Kohn energy band is used, while in Ref. 13, $V=0.6$ eV is used with $J=0.8$ eV and $W=4$ eV. In both cases, V is determined by requesting that for a single-impurity doping a bound state at $E_b=112$ meV appear as the combined result of the magnetic and Coulomb interactions. Our calculations indicate that the parameters of Ref. 20 provide an IB-VB crossover at $x_c \sim 0.5\%$ while we recovered the value $x_c \sim 3\%$ of Ref. 13 using the parameters that they provided. The discrepancy shows that the values assumed for W and J play an important role in the determination of V and x_c. The expression given by Benoit à la Guillaume *et al.*[24] provides an estimation of the nonmagnetic impurity potential that may include more than Coulomb interactions. It is evaluated using experimental data. For $x \approx 7\%$,[38,39] with $W=3$ eV and $J=1$ eV, we obtained the ratio $|V/J|=0.55$. The potential turns out to be repulsive, $V=-0.55$ eV. Notice that while the estimations of V performed for $x \to 0$ provide positive values, compatible with an attractive potential; the estimations at finite doping do not. As pointed out in the previous section, this indicates that it may be necessary to use an x-dependent expression for the nonmagnetic interactions.

The phenomenological potential proposed in Eq. (5) will provide an IB-VB crossover at $x \sim 0.1\%$ for all attractive values of V provided above, as seen in Fig. 2(b).

We can make estimations of x_c for (Ga,Mn)As and for other Mn-doped III-V materials as well. The value of J is expected to be inversely proportional to the volume of the cubic cell of the material a_0^3, according to the chemical trends, and the energy of the bound state for one Mn impurity has been measured.[23] Using these data we estimated V for different values of W, with the results given in Table I, which also includes a_0 for each material and the value of $a_B=\hbar/\sqrt{2m_k E_b}$, where $m_k=m_e/[\gamma_1-(6\gamma_3+4\gamma_2)/5]$ with m_e the electron mass and γ_i the Luttinger parameters.[40] Then x_0 can be obtained from Eq. (6) and it is also shown in the table. x_c ($\tilde{x}_c$)indicates the estimated values of the doping for which the IB-VB crossover occurs for an on-site (x-dependent) potential [$V(x)$ given by Eq. (5)].

It is clear that for all relevant values of x, (Ga,Mn)As is in the VB regime. The crossover, for realistic values of W, occurs at $x \lesssim 1\%$ for both on-site and x-dependent potentials. Thus, even including the Coulomb attraction, our results indicate that the IB regime is not expected to play a relevant role in this material. A similar picture emerges for (Ga,Mn)Sb. In this case the IB-VB crossover is expected to occur for such small values of impurity doping that for all practical purposes the Coulomb attraction can be neglected.

On the other hand, the IB regime seems to dominate the physics of (Ga,Mn)N. Considering $J=2.5$ eV, within our model we found that even for the largest value of W considered (namely, $W=10$ eV), J/W is strong enough to generate an IB region below some finite $x_c(W)$, even if no Coulomb attraction is considered. However, since the single-hole bound energy for GaN is 1.4 eV—i.e., much larger than the 0.113 eV value observed in GaAs—it is clear that the Coulomb-attraction term has to be incorporated. In the table

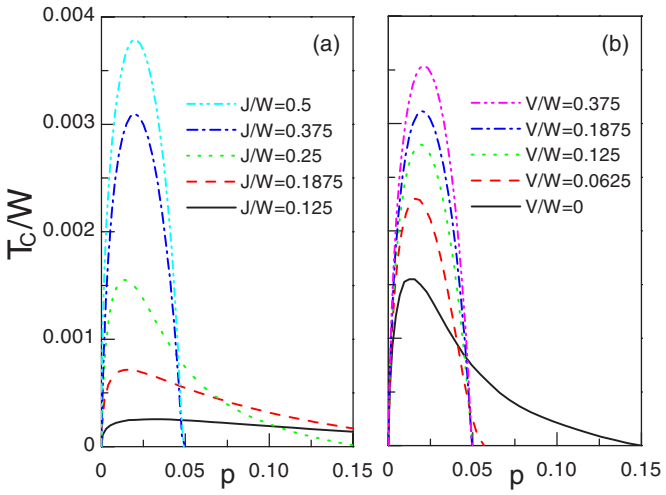

FIG. 3. (Color online) (a) T_C vs p at $V/W=0$ for several values of J/W. (b) T_C vs p at $J/W=0.25$ for various values of V/W. In both frames $x=0.05$.

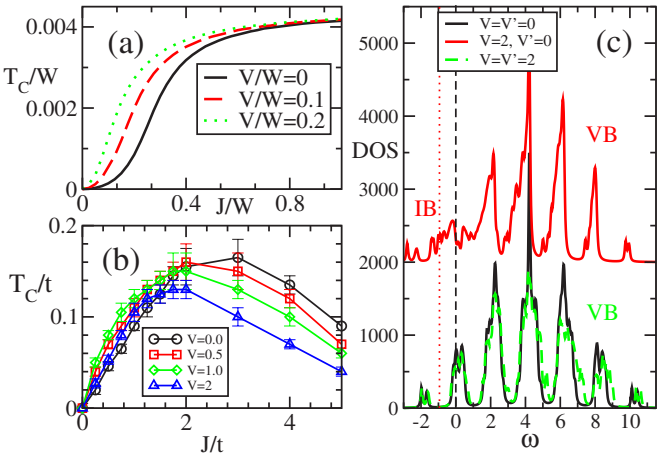

FIG. 4. (Color online) (a) T_C vs J/W at $p=0.015$ and $x=0.05$ calculated with DMFT for different values of V/W. (b) T_C vs J for different values of V at $p_h=0.3$ and $x=0.25$ obtained by MC simulations. (c) The MC obtained density of states (DOS) for $J/t=1$ and $V=0$ (black line), for an on-site Coulomb attraction $V=2$ (red line; the curve has been shifted vertically for clarity), and for a finite-range Coulomb attraction with on site intensity V and next-nearest-neighbor intensity V' $(=V=2)$ (dashed green line). The vertical lines indicate the chemical potential. For clarity, the curves for finite Coulomb attraction strength have been shifted along ω so that the central peak in the DOS of all the curves coincides.

we show the values of V that together with J will produce the bound state for different values of the bandwidth W. Our calculations show that with an on-site potential (Ga,Mn)N will be in the IB regime for all relevant values of x (we studied up to $x=80\%$). This is still true when an x-dependent V is considered since even in the case for the largest bandwidth considered the crossover is expected to occur at $x \approx 7.2\%$. Coulomb attraction should therefore be included to study this material.

Our results for (Ga,Mn)P indicate that despite the deeper position of the bound state in the gap, studies neglecting the Coulomb attraction could be performed, particularly for $x \gtrsim 3\%$.

For completeness, and to compare with previous calculations,[13] we present the T_C vs p dependence obtained from Eq. (4) at $x=0.05$, for different values of J's and no Coulomb attraction in Fig. 3(a). For $J/W \ll J_c/W$, T_C is low and almost independent of p. When $J/W > J_c/W$—i.e., in the IB regime—T_C vs p is semicircular with a maximum at $p=x/2$, in agreement with previous results for one-orbital models.[10] The behavior of T_C vs p at different values of V/W for $J/W=0.25$ is shown in Fig. 3(b). Comparing with the curves in part (a) of the figure it is clear that V increases the effective value of J. Our results agree with Ref. 13 and confirm that an on-site square-well V simply renormalizes J. The dependence of T_C on J for different values of V is shown in Fig. 4(a). V boosts T_C at small and intermediate J/W, while at large J/W's no change is observed because within DMFT the T_C saturates as $J \to \infty$. However, as will be discussed in the following section, we believe that the renormalization of J for the physically relevant values of x, such as the one used in our figures, is an artifact of the on-site range of the Coulomb attraction and, thus, we do not expect it to play a role in enhancing the T_C of real materials.

C. Monte Carlo simulations

Hamiltonian (1) was also studied here using a real-space MC technique with the Mn core spins treated classically. Details are not provided since the technique has been widely discussed before in the context of studies of manganites.[41] The simulations were performed using small cubic lattices with 4^3 sites at $x=0.25$. Finite-size effects are not strong as was shown by running some points on 5^3 clusters and obtaining similar results for T_C from the magnetization and spin-spin correlations versus temperature curves. However, the DOS reported below still preserves the spikes characteristic to finite-size systems. Nevertheless, the agreement with DMFT leads us to believe that the size effects must be mild in the MC simulations, although a detailed analysis of finite-size effects has not been carried out here. A random starting spin configuration has been selected as the starting point for each temperature T. The spins were allowed to evolve for a total of 10^5 MC steps, with the first 5×10^4 steps being discarded to thermalize the starting configuration.

At $J/t=1$ and $p_h=p/x=0.3$, a value $V/t=1$ for the on-site Coulomb attraction increases T_C by as much as 33%, as shown in Fig. 4(b). This agrees qualitatively with the DMFT results. The figure shows clearly how V effectively "renormalizes" J. Since the curve T_C vs J for $V=0$ has a maximum at J^{max}, the effect of V is to increase T_C for values of $(J+V) \lesssim J^{max}$, while T_C decreases with V for values of $(J+V) \gtrsim J^{max}$. Although this renormalization has been previously reported,[13] we do not believe that it will play a role in the relevant range of doping for most DMSs. As we pointed out in Sec. IV A, the on-site range of the Coulomb attraction induces unphysical behavior by exaggerating hole localization for values of x for which overlap of the hole wave functions should occur. While finite-range attraction cannot be studied with DMFT, it can be studied with MC simulations but at the price of not being able to access the low-doping

regime at which the IB-VB crossover would be expected to occur for a material such as (Ga,Mn)As.

In Fig. 4(c), we present the DOS obtained with MC for $J/t=1$ and $V=0$ for $x=25\%$ indicated by the black solid line. The peaks are due to the finite size of the system, and each of them can be identified with the spikes that appear in the DOS of a noninteracting system in the same lattice. Thus, at this value of J, there is only a VB in the DOS; i.e., the magnetic interaction is not strong enough to develop an impurity band. The position of the chemical potential μ is indicated by the black dashed line. Upon adding an on-site Coulomb attraction $V/t=2$, we observe that an IB develops as indicated by the red line in the figure, which has been shifted upwards along the vertical axis for clarity. This IB is due to the localization of the holes induced by the on-site potential. The criterion used to determine that the DOS has an IB at $V/t=2$ on a finite lattice is based on the appearance of weight right below the chemical potential in a location that carries negligible weight at $V=0$. The chemical potential denoted by the dotted red line indicates that only states in the IB are occupied. However, when the range of the potential is increased to next-nearest neighbors, as indicated by the green dashed line in the figure, it can be seen that the IB disappears although the intensity of the potential has not changed. This occurs because, at this large doping, the extended potential allows for a more uniform distribution of the holes. As can be seen in the figure, the DOS for $V=0$ and for finite extended V have an almost perfect overlap. This shows that the use of an on-site Coulomb attraction potential can lead to misleading results and the authors have to be cautious when using this approximation.

V. CONCLUSIONS

Our combined DMFT-MC study shows that the Coulomb attraction by acceptors needs to be considered to obtain correctly the IB-VB crossover as a function of impurities concentration x in models of DMSs. However, for most materials we find that the crossover occurs at very low levels of doping, outside the regime in which high T_C would be expected. We also find that a doping-independent on-site square-well potential acts as a renormalization of the coupling J in an extended doping range up to $x=80\%$. However, this apparent boost to the J term at all Mn dopings is unphysical, since the effect of V should be x dependent beyond some critical value. Our MC simulations shows that this x dependence is achieved naturally by considering a longer-range (next-nearest-neighbor) square-well attraction, which is beyond the capability of the DMFT which can deal with on-site interactions only. Thus, a phenomenological x-dependent Coulomb attraction was introduced. With this modification, we have shown that for (Ga,Mn)As, the Coulombic attraction V influences the physics of the material only at small Mn doping—i.e., $x \lesssim 0.5\%$. This result shows that it is correct to apply theories that consider the J term only for studying the properties, including the Curie temperature, of (Ga,Mn)As at the relevant values of Mn concentrations $x \sim 1\%$–10%. On the other hand, we found that the Coulomb attraction will play a relevant role, and should be included, in studies of Mn-doped GaN.

Summarizing, here we have shown that the addition of an attractive Coulomb potential is the necessary ingredient to explain the transition from the IB to the VB regime as a function of Mn impurity concentration in materials for which the magnetic interaction J is not strong enough to bind a hole. However, we find that, except for the case of (Ga,Mn)N, the crossover occurs at very low doping in a regime in which high ferromagnetic critical temperatures would not be expected and, thus, the effective value of J will not be affected. As a consequence, it is not necessary to include the Coulomb attraction in the calculations. In addition, we show that an on-site attractive potential does not capture the overlap of localized hole wave functions that should occur as a function of doping and it provides unphysical results. Thus, to study materials such as (Ga,Mn)N, in which the Coulomb attraction is relevant, a nearest-neighbor finite-range potential has to be used.

ACKNOWLEDGMENTS

We acknowledge helpful discussions with T. Dietl and J. Sinova. This research was supported in part by the National Science Foundation Grants No. DMR-0443144 and No. DMR-0454504 and also in part by the Division of Materials Sciences and Engineering, Office of Basic Energy Sciences, U.S. Department of Energy, under Contract No. DE-AC05-00OR22725 with ORNL, managed by UT-Battelle.

*florentin_p@hotmail.com

[1] I. Žutić, J. Fabian, and S. Das Sarma, Rev. Mod. Phys. **76**, 323 (2004).

[2] H. Ohno, Science **281**, 951 (1998); T. Jungwirth, J. Sinova, J. Maček, J. Kučera, and A. H. MacDonald, Rev. Mod. Phys. **78**, 809 (2006); A. H. MacDonald, P. Schiffer, and N. Samarth, Nat. Mater. **4**, 195 (2005).

[3] T. Dietl, H. Ohno, F. Matsukura, J. Cibert, and D. Ferrand, Science **287**, 1019 (2000).

[4] M. Abolfath, T. Jungwirth, J. Brum, and A. H. MacDonald, Phys. Rev. B **63**, 054418 (2001).

[5] M. Berciu and R. N. Bhatt, Phys. Rev. Lett. **87**, 107203 (2001); H. Akai, *ibid.* **81**, 3002 (1998).

[6] S. J. Potashnik, K. C. Ku, S. H. Chun, J. J. Berry, N. Samarth, and P. Schiffer, Appl. Phys. Lett. **79**, 1495 (2001).

[7] K. C. Ku, S. J. Potashnik, R. F. Wang, S. H. Chun, P. Schiffer, N. Samarth, M. J. Seong, A. Mascarenhas, E. Johnston-Halperin, R. C. Myers, A. C. Gossard, and D. D. Awschalom, Appl. Phys. Lett. **82**, 2302 (2003).

[8] K. S. Burch, D. B. Shrekenhamer, E. J. Singley, J. Stephens, B. L. Sheu, R. K. Kawakami, P. Schiffer, N. Samarth, D. D. Awschalom, and D. N. Basov, Phys. Rev. Lett. **97**, 087208 (2006).

[9] J. Okabayashi, A. Kimura, O. Rader, T. Mizokawa, A. Fujimori, T. Hayashi, and M. Tanaka, Phys. Rev. B **64**, 125304 (2001); Physica E (Amsterdam) **10**, 192 (2001).

[10] One-band models with the exact diagonalization of the Hamiltonian were studied in G. Alvarez, M. Mayr, and E. Dagotto, Phys. Rev. Lett. **89**, 277202 (2002) and M. Mayr, G. Alvarez, and E. Dagotto, Phys. Rev. B **65**, 241202(R) (2002). In M. P. Kennett, M. Berciu, and R. N. Bhatt, *ibid.* **66**, 045207 (2002), the IB band model was numerically analyzed. Combined mean-field and percolative ideas were used in S. Das Sarma, E. H. Hwang, and A. Kaminski, *ibid.* **67**, 155201 (2003). MC results for the kinetic-exchange model are in J. Schliemann, Jürgen König, and A. H. MacDonald, *ibid.* **64**, 165201 (2001), and LSDA estimations of T_C are in J. L. Xu, M. van Schilfgaarde, and G. D. Samolyuk, Phys. Rev. Lett. **94**, 097201 (2005).

[11] F. Popescu, Y. Yildirim, G. Alvarez, A. Moreo, and E. Dagotto, Phys. Rev. B **73**, 075206 (2006).

[12] R. S. Fishman and M. Jarrell, J. Appl. Phys. **93**, 7148 (2003); R. S. Fishman, J. Moreno, T. Maier, and M. Jarrell, Phys. Rev. B **71**, 180405(R) (2005); R. S. Fishman, F. Popescu, G. Alvarez, T. Maier, J. Moreno, and M. Jarrell, New J. Phys. **8**, 116 (2006).

[13] M. Takahashi and K. Kubo, J. Phys. Soc. Jpn. **72**, 2866 (2003).

[14] E. H. Hwang and S. Das Sarma, Phys. Rev. B **72**, 035210 (2005).

[15] J. Okabayashi, A. Kimura, O. Rader, T. Mizokawa, A. Fujimori, T. Hayashi, and M. Tanaka, Phys. Rev. B **58**, R4211 (1998).

[16] Y. Yildirim, G. Alvarez, A. Moreo, and E. Dagotto, arXiv:cond-mat/0612002 (unpublished).

[17] J. Schneider, U. Kaufmann, W. Wilkening, M. Baeumler, and F. Köhl, Phys. Rev. Lett. **59**, 240 (1987).

[18] R. A. Chapman and W. G. Hutchinson, Phys. Rev. Lett. **18**, 443 (1967).

[19] T. Frey, M. Maier, J. Schnaider, and M. Gehrke, J. Phys. C **21**, 5539 (1988).

[20] A. K. Bhattacharjee and C. B. à la Guillaume, Solid State Commun. **113**, 17 (2000). $E_b^{(pd)}(E_b^{(C)}) \sim 26.25(86.15)$ meV.

[21] J. Tworzydlo, Phys. Rev. B **50**, 14591 (1994).

[22] T. Dietl, arXiv:cond-mat/0703278 (unpublished).

[23] T. Dietl, F. Matsukura, and H. Ohno, Phys. Rev. B **66**, 033203 (2002).

[24] C. Benoit à la Guillaume, D. Scalbert, and T. Dietl, Phys. Rev. B **46**, 9853 (1992).

[25] E. H. Hwang, A. J. Millis, and S. Das Sarma, Phys. Rev. B **65**, 233206 (2002).

[26] M. J. Calderón, G. Gómez-Santos, and L. Brey, Phys. Rev. B **66**, 075218 (2002).

[27] S.-R. Eric Yang and A. H. MacDonald, Phys. Rev. B **67**, 155202 (2003).

[28] S. Pantelides, Rev. Mod. Phys. **50**, 797 (1978).

[29] Ideally a potential with a finite range up to next-nearest neighbors should be used but its implementation is beyond the capabilities of DMFT.

[30] E. Müller-Hartmann, Z. Phys. B: Condens. Matter **74**, 507 (1989); **76**, 211 (1989); W. Metzner and D. Vollhardt, Phys. Rev. Lett. **62**, 324 (1989).

[31] For a review of DMFT, see A. Georges, G. Kotliar, W. Krauth, and M. J. Rozenberg, Rev. Mod. Phys. **68**, 13 (1996).

[32] The average $\langle X(\mathbf{m})\rangle = \int d\Omega_{\mathbf{m}} X(\mathbf{m}) \mathcal{P}(\mathbf{m})$ is over the orientations $\mathbf{m}$ of the local moment on site 0 and is a matrix in 2×2 spin space; $\mathcal{P}(\mathbf{m})$ is the probability for the local moment to point in the $\mathbf{m}$ direction. While $\mathcal{P}(\mathbf{m}) = 1/4\pi$ above T_C (Ref. 12), in the FM phase near T_C, $\mathcal{P}(\mathbf{m}) \propto \exp(-3\beta T_C M \mathbf{m})$ [see M. Auslender and E. Kogan, Phys. Rev. B **65**, 012408 (2001); E. Kogan and M. Auslender, *ibid.* **67**, 132410 (2003); M. Auslender and E. Kogan, Europhys. Lett. **59**, 277 (2002)], where $\beta = 1/T$ and $M = \langle m_z \rangle_{\mathbf{m}} \in [0,1]$ is the local-moment order parameter. While $M = 1$ deeply in the FM state, at the transition $M = 0$. $\hat{\mathbf{I}}$ is the unity matrix.

[33] N. Furukawa, J. Phys. Soc. Jpn. **63**, 3214 (1994); **64**, 2754 (1995); **64**, 3164 (1995).

[34] At the FM transition $B_+ = B_- \equiv B$, thus $\mathrm{DOS}_+(\omega) = \mathrm{DOS}_-(\omega)$ and the total $\mathrm{DOS} = -2\mathrm{Im}[B(\omega)]/\pi$.

[35] The behavior displayed in Fig. 2(a) was observed up to $x \approx 80\%$, i.e., a percentage of impurity doping well beyond the experimental possibilities. As x approaches 100% the crossover is difficult to monitor because in this limit the system would develop antiferromagnetic long-range order and the valence band is split in two subbands.

[36] Y. Yildirim *et al.* (unpublished).

[37] The Mott criterion states that upon doping a semiconductor a MIT occurs when the wave functions of the holes localized around the impurities start to overlap. This occurs when $n_{\mathrm{Mn}}^{1/3} a_B \sim 0.25$. n_{Mn} is the Mn density per unit volume and a_B is the Bohr radius of the hydrogenic impurity. Thus, we can obtain the relative concentration x_0 of Mn for which the wave functions would start to overlap in (Ga,Mn)As as $x_0 = n_{\mathrm{Mn}}/n_{\mathrm{Ga}}$, where the number of Ga ions per unit volume, $n_{\mathrm{Ga}} = 4/a_0^3$. Hence, Mott's criterion becomes $(4x_0/a_0^3)^{1/3} a_B = 0.25$.

[38] J. I. Hwang, Y. Ishida, M. Kobayashi, H. Hirata, K. Takubo, T. Mizokawa, A. Fujimori, J. Okamoto, K. Mamiya, Y. Saito, Y. Muramatsu, H. Ott, A. Tanaka, T. Kondo, and H. Munekata, Phys. Rev. B **72**, 085216 (2005).

[39] J. Okabayashi, A. Kimura, T. Mizokawa, A. Fujimori, T. Hayashi, and M. Tanaka, Phys. Rev. B **59**, R2486 (1999).

[40] P. Yu and M. Cardona, *Fundamentals of Semiconductors*, 3rd ed. (Springer-Verlag, Berlin, 2001).

[41] For an overview on manganites see E. Dagotto, T. Hotta, and A. Moreo, Phys. Rep. **344**, 1 (2001); E. Dagotto, *Nanoscale Phase Separation and Colossal Magnetoresistance* (Springer, Berlin, 2003).